Multiple stable states in hydrological models: An ecohydrological investigation

T. J. Peterson,[1] R. M. Argent,[2] A. W. Western,[1] and F. H. S. Chiew[3]

Received 31 January 2008; revised 12 August 2008; accepted 23 October 2008; published 7 March 2009.

[1] Many physical-based models of surface and groundwater hydrology are constructed without the possibility of multiple stable states for the same parameter set. For such a conceptualization, at the cessation of a transient hydrological disturbance of any magnitude the model will return to the same stable state and thus show an infinite resilience. To highlight and falsify this assumption, a numerical distributed ecohydrological model (coupled hillslope Boussinesq-vertically lumped vadose zone) is presented, in which qualitatively different steady state water table elevations exist for the same parameter set. The multiple steady states are shown to emerge from a positive feedback arising from a reduction in leaf area index (LAI) and thus transpiration, as a saline water table approaches the surface. Limit cycle continuation is also undertaken to quantify the state-space location of the threshold (repellor) between the steady states (attractors) and quantify the resilience. While the model is biophysically simple, it is sufficiently complex to challenge this potentially significant assumption within water resource planning.

Citation: Peterson, T. J., R. M. Argent, A. W. Western, and F. H. S. Chiew (2009), Multiple stable states in hydrological models: An ecohydrological investigation, *Water Resour. Res.*, *45*, W03406, doi:10.1029/2008WR006886.

1. Introduction

[2] Many physical based models of surface and groundwater hydrology are constructed without thought given to the possibility of multiple stable states for the same parameter set. For such a conceptualization, at the cessation of a transient hydrological disturbance of any magnitude the model will return to the same stable state, and thus show an infinite resilience. In an attempt to make this assumption less implicit, a numerical hydrological model is presented in which this assumption is violated.

[3] The impetus for the model derives from the concept of ecosystem resilience (referred to henceforth as resilience) [*Walker et al.*, 2004]. It is a concept, derived from dynamic systems theory, in which biophysical environments are investigated for multiple possible equilibrium (henceforth generalized to the term *attractor*) for the same parameters [*Ludwig et al.*, 1997; *Holling*, 1973]. Within the hydrological and water resource management literature consideration of the prevalence, relevance or possibility of multiple attractors is very minimal. The existing literature comprises a discussion of the potential significance of multiple hydrological attractors by *Dent et al.* [2002]; qualitative agricultural case studies [*Allison*, 2003; *Allison and Hobbs*, 2004; *Walker et al.*, 2002]; arid-climate one-dimensional soil moisture models of multiple equilibria, or modes, resulting from assumptions of multiequilibrium landcover [e.g., *Walker et al.*, 1981; *D'Odorico et al.*, 2005; *van de Koppel and Rietkerk*, 2004; *von Hardenberg et al.*, 2001]; rainfall recycling producing multiple soil moisture modes [e.g., *Charney and Stone*, 1974; *D'Odorico and Porporato*, 2004], and a simple nonbiophysical one-dimensional water table model presenting multiple hydrological attractors [*Ridolfi et al.*, 2006]. The soil moisture and rainfall recycling investigations cited above do explicitly investigate multiple hydrological attractors, though at a scale of questionable relevance to water resource management. The rainfall recycling positive feedback is proposed to operate at the subcontinental scale, while the arid-climate soil moisture feedback has been investigated only at the subplot scale. The only significant quantitative catchment scale hydrological resilience model is of *Anderies* [2005] and its extensions: *Peterson et al.* [2005] and *Anderies et al.* [2006]. The *Anderies* [2005] model is an annual time step, salt and water storage, groundwater-vadose zone lumped model of the Goulburn catchment (Victoria, Australia). It predicts the region to have two attractors: a near surface water table and a deep water table. As a result of widespread land clearing the deep water table attractor is predicted to have been lost with only the near surface water table attractor remaining. See *Peterson et al.* [2005] for a more detailed critique.

[4] Examples within the hydrological literature of an explicit assumption of a single attractor could not be found. Models in which a steady state solution is independent of the initial conditions does though provide examples in which two attractors cannot exist. Such models include ModFlow-2000 [*Harbaugh et al.*, 2000], Flowtube, a one-dimensional Boussinesq equation-based groundwater model [*Argent et al.*, 2001], and a one-dimensional soil moisture model [*Laio et al.*, 2001]. For rainfall-runoff models, such

[1]Department of Civil and Environmental Engineering, University of Melbourne, Parkville, Victoria, Australia.
[2]Water Division, Bureau of Meteorology, Melbourne, Victoria, Australia.
[3]CSIRO Land and Water, Canberra, ACT, Australia.

0043-1397/09/2008WR006886

as Topmodel [*Beven and Kirkby*, 1979] or SIMHYD [*Chiew et al.*, 2002], the fluxes are of interest rather than the comparably slow groundwater state variables and, as such, steady state solutions are very rarely sought. However, a single attractor can be inferred by the return of the output hydrograph to that of the predisturbance hydrograph for any magnitude disturbance, assuming the pre and postdisturbance climatic forcing is identical. A second illustration of the assumption of one attractor is found in the low significance given to initial conditions in transient simulations. For transient groundwater modeling, this is often shown with the solution starting from a plausible initial state, rather from a state chosen through investigation of responses to different initial conditions [e.g., *Beverly et al.*, 1999]. With lumped rainfall-runoff models, such as SIMHYD, initial conditions are often arbitrarily assigned and simulations undertaken with an initial warm-up period to minimize their significance to the period of interest. With the exception of the study of *Ridolfi et al.* [2006], a final illustration is found in the lack of use of continuation analysis to investigate multiple attractors (see section 3.2 for a description of continuation analysis).

[5] While the concepts of resilience and multiple attractors are worthy of inquiry, resilience models are almost always theoretical studies that are not calibrated or validated against observed data. While it is questionable whether an unobserved attractor can be numerically validated via data from the observed attractor, calibration of the model to the observed attractor is thought a necessary first step. As per *Anderies* [2005], this paper investigates vadose-hydrogeological interactions. The focus here is on the development of a rigorous biophysical model for the exploration of multiple attractors and future calibration. The model is therefore developed so that (1) the number of parameters and state variables are minimal; (2) where possible, parameters are independently observable; and (3) it is spatially distributed to aid calibration to observed groundwater levels. This is achieved using a modified hillslope Boussinesq groundwater equation coupled with a vertically lumped one-dimensional vegetation-vadose zone model.

2. Model Development

[6] The model is developed from the assumption that multiple coexistent hydrological attractors do not exist. The aim is not to prove that such attractors exist but rather that minor, defensible and plausible changes to modeling of groundwater-vadose zone interactions can give rise to multiple attractors. That is, the paper aims to falsify the assumption that dryland catchments only have a single hydrologic attractor.

[7] The following coupled model is not aiming to improve the validity or predictive accuracy of existing coupled models. It is developed to tractably explore the potential for multiple attractors within the parameter space. To explore the state-space location of thresholds between attractors (henceforth generalized to the term *repellor*) also requires the model to have a smooth and continuous response surface, without the thresholds caused by, for example, min/max and if/else functions. This also reduces the stiffness of the differential equations and facilitates the future use of gradient-based calibration. As a compromise between the high frequency soil moisture dynamics and the low frequency lateral groundwater flow, the model time step is monthly. Central to the model is the interaction between transpiration and the water table. Until recently ecohydrological investigations focused upon water-limited ecosystems in which interaction of the vadose zone with the water table was omitted [*Rodriguez-Iturbe et al.*, 2007]. *Rodriguez-Iturbe et al.* [2007] recently stressed the importance of development of a framework to investigate interaction of the water table, soil moisture, rainfall regime, and vegetation. Subsequently, the interaction of bare soil and a shallow water table with stochastic rainfall was investigated, although this was limited to one-dimensional vertical flow [*Ridolfi et al.*, 2008]. The model developed here addresses some of the unresolved issues by *Rodriguez-Iturbe et al.* [2007], namely redistribution via lateral saturated flow and vegetation, and demonstrates that complex behavior can arise from a relatively simple model.

[8] Figure 1 summarizes the model developed over the following pages. It presents the model as a cross section over the catchment length with an inset summarizing the unsaturated zone model. Lateral flow occurs only within the saturated zone and the flow direction is perpendicular to the aquifer-basement boundary. Saturated flow can occur in both the aquifer and soil layers, if the water table is within the soil layer. The depth of the unsaturated layer is the minimum of the depth to the lower soil layer boundary and the depth to the water table. With respect to the inset, the unsaturated zone is vertically lumped and rainfall is partitioned to runoff and infiltration. Unsaturated fluxes are assumed vertical and, if the water table is within the soil layer, both recharge to and uptake from the groundwater can occur.

[9] Numerous other coupled vadose-lateral groundwater models have been developed. A notable early model was a rigorous full hydraulic head-based three-dimensional, vertically discretized, transient model [*Freeze*, 1971]. Aiming to overcome the computational load, many hillslope hydrology models have subsequently simplified Richard's equation [e.g., *Kim et al.*, 1999; *Hilberts et al.*, 2007]. Within groundwater modeling, coupled models have also emerged [e.g., *Barlow and Harbaugh*, 2006; *Niswonger et al.*, 2006; *Cordano and Rigon*, 2008]. Differences between the following model and the above-cited hillslope models include vertically integrated unsaturated zone; time steps of one month compared to predominately subdaily time steps; and the transpiration being a function of both depth to water table and soil moisture, rather than soil moisture alone. With respect to the cited groundwater models, the following model is only one-dimensional, has one layer and only has saturated lateral flow. The model does, however, partition rainfall to runoff and infiltration, and utilizes pressure head gradient vadose zone drainage. Such dynamics are not required to achieve the presented dynamics but are included (1) as their omission would require assumptions potentially invalidating the findings and (2) to facilitate future field application of the model. Discretizing the soil layer was also investigated, and was found to increase the memory requirements of the limit cycle continuation sparse Jacobian matrix significantly beyond the 8-GB capacity of 64-bit desktop computers, and was thus considered premature.

2.1. Ecohydrological Model

[10] Field studies of vadose zone-water table interaction emerge predominately from Australian salinity management investigations. For irrigated lucerne with a 1-m deep water

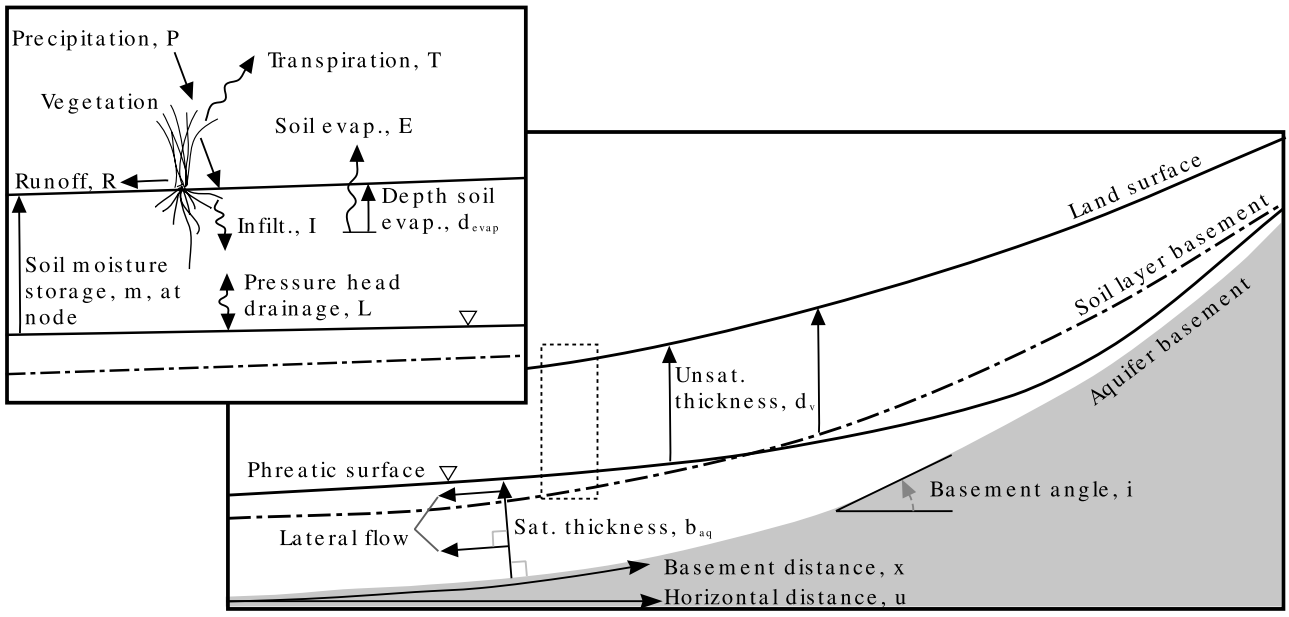

Figure 1. Schematic of the coupled model. (top left) Inset details the one-dimensional unsaturated zone model.

table, a two-site lysimeter study found that with a change from fresh (0.1 dS m^{-1}) to saline (16 dS m^{-1}) water table, the leaf area index (LAI) declined by 41%; transpiration by 36%; and groundwater uptake by 67% [*Zhang et al.*, 1999]. Uptake from the saline groundwater was estimated, at each site, at 3.3 and 2.3 mm day^{-1}, of which 19% (0.21 and 0.15 mm day^{-1}, respectively) was estimated to be transpired. Summarizing 20 field studies, *Thorburn* [1997] concluded that, following establishment of trees and pastures, groundwater uptake of shallow saline groundwater by each is very comparable to that of bare soil. A further study of 80 woody revegetation sites found that groundwater uptake is minor at sites with shallow saline water tables, and observed lowering of the water level is likely to be due to initial direct uptake followed by reduced in situ recharge [*George et al.*, 1999]. With respect to field studies of tree water use, an in situ investigation of *Eucalyptus largiflorens* found that at sites recharged only by vertical infiltration, uptake was from fresh unsaturated deep drainage rather than accessible saline groundwater [*Holland et al.*, 2006]. Conversely, *Thorburn et al.* [1993] concluded groundwater uptake was an important source but acknowledged that a high saline water table may have restricted transpiration and uptake. Returning to plant growth, the leaf area per tree of *E. camaldulensis* and *E. occidentalis* after a 7-year growth was found to decrease by 50% and 61%, respectively, at sites of moderately saline shallow groundwater compared to fresh sites [*Benyon et al.*, 1999].

[11] Although these studies differ in location (and thus climate, geology, soil), species, method and aims, it is plausible to summarize that (1) transpiration declines as a shallow saline water table intersects a greater fraction of the root zone; (2) the reduction in transpiration is coupled with a reduction in LAI; and (3) uptake of saline groundwater by pastures and eucalyptus is a minimal fraction of their total transpiration. This forms the basis for the modified transpiration function in the following model development.

[12] In the development of the monthly time step model, the monthly change in soil moisture cannot be assumed zero and thus soil moisture state variables are required. As this investigation is into long-term multiple equilibrium of the water table rather than soil moisture dynamics, the soil moisture is vertically integrated to a single layer store. The surface slope is assumed sufficiently flat that lateral unsaturated flow is also zero. The unsaturated zone point water balance is thus:

$$\frac{dm(x,t)}{dt} = I(m,S,t) - E(m,S,t) - T(m,S,t) - L(m,S) - U(m,S) \quad (1)$$

where m [L] is soil moisture at time t [T] and at a distance x [L] from the catchment outlet; S [L^2] is groundwater storage per unit length; I [$L\,T^{-1}$] is infiltration rate; E [$L\,T^{-1}$] is soil evaporation rate; T [$L\,T^{-1}$] is transpiration rate; L [$L\,T^{-1}$] is leakage to, or uptake from, the water table; and U [$L\,T^{-1}$] is uptake (deposition) of soil moisture as a result of a rising (lowering) water table.

[13] In partitioning rainfall for infiltration, the interception storage capacity was estimated from the LAI and assumed to empty daily [*Wigmosta et al.*, 1994; *Dickinson et al.*, 1991]. The effective rainfall, P_{eff} (in meters), and the maximum rainfall to infiltration, P_{infilt} [$L\,T^{-1}$], is thus:

$$P_{eff} = P - 10^{-4} LAI_t \times F \quad (2)$$

$$P_{infilt} = \min\left(P_{eff}, m_{\max} - m\right) \approx P_{eff} - \lambda_P \ln\left[e^{\frac{P_{eff}-(m_{\max}-m)}{\lambda_P}} + 1\right] \quad (3)$$

where LAI_t is the dimensionless leaf area index at time t (equation (7)); F is ground cover fraction of the canopy, which as per *Tuteja et al.* [2004] is assumed to equal unity; and λ_P [L] is a smoothing parameter for approximating the

above min function [*Kavetski and Kuczera*, 2007], trials for which identified acceptable smoothing to occur when λ_P = 0.005 m; and $m_{\max}$ [L] is the maximum soil moisture capacity equal to the soil porosity, ϕ, multiplied by the minimum of the vertical depth of the soil layer and the depth to the water table (or depth below natural surface, DBNS), d_v [L]. The infiltration rate, I, is estimated from the study of *Yu et al.* [1997] by:

$$I = I_p\left(1 - e^{-\frac{P_{infilt}}{I_p}}\right) \tag{4}$$

$$I_p = I_o e^{\frac{m_{\max} - m}{m_{\max}}} \tag{5}$$

where I_p [L T^{-1}] is the spatially averaged potential infiltration rate; and I_o [L T^{-1}] is a parameter for the spatially averaged limiting infiltration rate when saturation occurs over the entire cell, generating runoff [*Tuteja et al.*, 2004].

[14] Three fluxes are simulated from the soil moisture store: evaporation, transpiration and nonfree draining leakage to the water table. Transpiration is frequently modeled as a piecewise linear function of the soil moisture fraction multiplied by the potential evapotranspiration [e.g., *Laio et al.*, 2001]. Above a soil moisture fraction designated θ_*, the sum of transpiration and soil evaporation is at the rate of potential evapotranspiration. For long-term simulations though, the potential transpiration is also a function of vegetation growth and seasonality. A simple model incorporating both is the linear piecewise soil moisture function multiplied by an estimate of the potential transpiration. The later was derived from scaling potential evaporation by one minus the exponential function of *Monsi and Saeki* [2005] for relative shaded light intensity as a function of LAI [implemented within *Vaze et al.*, 2004]. Transpiration was estimated thus as:

$$T = PET\left(1 - e^{-k_{light}LAI_t}\right)\Theta_{TF} \tag{6}$$

where PET [L T^{-1}] is the areal potential evapotranspiration; k_{light} is the dimensionless canopy light extinction coefficient; LAI$_t$ is the dimensionless leaf area index at time t; and $0 \le \Theta_{TF} \le 1$ is the linear piecewise function.

[15] The discussion above of the impact of a shallow saline water table on vegetation transpiration clearly indicates that transpiration and LAI decline with both increasing groundwater salinity and rising water table. A simple further modification is to make LAI, and thus transpiration, a function of DBNS. That is, as the water table lowers from the surface to far below the root zone the LAI increases from zero to a predefined climatic maximum. Multiplying the equation for LAI$_t$ by *Tuteja et al.* [2004] by a two-parameter polynomial logistic function results in LAI$_t$ being a function of both rainfall and DBNS:

$$LAI_t = LAI_{month}\left(\frac{P}{P_i}\right)^{\beta}\left(\frac{d_v^{\alpha}}{d_v^{\alpha} + d_{LAI/2}^{\alpha}}\right) \tag{7}$$

where LAI$_{month}$ is the fixed average monthly LAI; P_i [L T^{-1}] is the average monthly rainfall for month i; β is a scaling parameter for the change in LAI with the rainfall ratio; $d_{LAI/2}$ [L] is a parameter for the water table depth at which the LAI is 50% of the maximum; and α is a parameter for the LAI rate of decay as the water table rises. The logistic function aggregates a reduction in transpiration from an increase in soil salinity, due to both reduced osmotic potential and the toxicity of salt to vegetation. It thus ignores changes in vegetation sensitivity to salt with growth and season. Soil salt flushing from, and uptake to, the root zone is also ignored. Effectively, at each time step the soil salinity is assumed to be in a quasiequilibrium.

[16] The Θ_{TF} of equation (6) is often estimated as a linear piecewise function in which the transpiration potential fraction equals zero below a wilting point, and increases linearly to unity at and above the soil moisture level where plant stomata being to close. To eliminate the thresholds at the wilting and stomata closure points, the integral of the smooth step function by *Kavetski and Kuczera* [2007] was expanded to include smoothing of two thresholds:

$$\Theta_{TF} = \frac{\lambda_\theta}{\theta_* - \theta_{wp}} \ln\left(\frac{1 + e^{\frac{\theta - \theta_{wp}}{\lambda_\theta}}}{1 + e^{\frac{\theta - \theta_*}{\lambda_\theta}}}\right) \tag{8}$$

where θ_{wp} is a dimensionless parameter for the vegetation wilting point soil moisture fraction; θ_* is a dimensionless parameter for the soil moisture fraction at which stomata begin to close as a result of water stress; θ is the dimensionless soil moisture fraction defined as the soil moisture store, m, over the unsaturated depth, d_v, and approximated by the smooth function of equation (10); and λ_θ is a dimensionless parameter affecting smoothing, trials for which identified acceptable smoothing to occur when λ_θ = 0.001.

[17] The estimation of evaporation, E, below is comparable to transpiration except that (1) the relative evaporation fraction, Θ_{EF}, is extended to the soil moisture residual and porosity and (2) only the upper soil column is available for evaporation:

$$E = PETe^{-k_{light}LAI_t}\Theta_{EF}\delta_E \tag{9}$$

where $0 \le \Theta_{EF} \le 1$ is the relative evaporation fraction; and $0 \le \delta_E \le 1$ is the fraction of the soil column available for surface evaporation. The relative evaporation fraction, Θ_{EF}, is estimated from a smooth function for θ that approximates $\frac{m}{d_v}$ and is comparable to the relative transpiration fraction of equation (8):

$$\theta = \frac{m}{d_v} \approx \theta_r + \lambda_\theta \ln\left(\frac{1 + e^{\frac{\frac{m}{d_v} - \theta_r}{\lambda_\theta}}}{1 + e^{\frac{\frac{m}{d_v} - \phi}{\lambda_\theta}}}\right) \tag{10}$$

$$\Theta_{EF} = \frac{\theta - \theta_r}{\phi - \theta_r} \tag{11}$$

where θ_r is a dimensionless parameter for the soil moisture residual and ϕ is a dimensionless parameter for the soil porosity. In estimating δ_E, it is reasonable to assume the fraction of potential evaporation at a depth, d, from a soil layer declines from unity at the surface and approaches zero as d extends far below the land surface. Assuming exponential decay at a rate of a, δ_E is estimated from its integral over a depth from zero to d_v by:

$$\delta_E = \frac{1}{a}\left(1 - e^{-ad_v}\right) \tag{12}$$

where

$$a = -\frac{\ln \Gamma}{d_{evap}} \tag{13}$$

where d_{evap} [L] is a parameter for the soil depth at which the fraction of potential evaporation equals Γ, a dimensionless constant which in this application was fixed at 0.05.

[18] In estimating the leakage to the water table, L, most integrated soil moisture models assume the water table is sufficiently below the root zone that leakage can be estimated as free draining [e.g., *Laio et al.*, 2001]. The inclusion herein of a water table thus requires the total vertical vadose zone hydraulic head to include the pressure potential in addition to the elevation head. From Darcy's equation and assuming the drainage is quasisteady state, the leakage is estimated as:

$$L = -k_\theta \left(\frac{\partial \psi}{\partial z} + 1 \right) \tag{14}$$

where k_θ [L T^{-1}] is the unsaturated vertical hydraulic conductivity; ψ [L] is the pressure potential; and z is the upward positive elevation. In estimating $\frac{\partial \psi}{\partial z}$, the partial derivatives of the osmotic, bulk and pressure potentials are assumed zero, and is approximated by only the matric potential. Estimating the matric potential, ψ_m, from the center of the unsaturated zone, and assuming the matric potential is zero at the water table, gives:

$$\begin{aligned} \frac{\partial \psi}{\partial z} &= (S < S_{aq}) \frac{\partial \psi_m}{\partial z} \\ &\approx (S < S_{aq}) \frac{\psi_m - 0}{0.5 d_v - 0} \\ &\approx 2\lambda \frac{\psi_m}{d_v} \end{aligned} \tag{15}$$

where S_{aq} [L^2] is the groundwater storage capacity below the lower soil boundary (see equation (22)); $(S > S_{aq})$ is a nonsmooth step function equaling zero when $S \leq S_{aq}$ and one when $S > S_{aq}$. To smoothen the above finite difference approximation, a dimensionless function λ is adopted. It is an infinitely differentiable logistic function approximating the discontinuous step function $(S > S_{aq})$ [*Kavetski and Kuczera*, 2007]:

$$\lambda = \frac{1}{1 + e^{\frac{S - S_{aq}}{\lambda_S}}} \tag{16}$$

λ_S [L^2] is a smoothing parameter. To ensure a smooth behavior near saturation, ψ_m and k_θ were estimated from *van Genuchten* [1980] and thus require the following parameters: air entry pressure, ψ_a [L]; maximum vertical conductivity, k_v [L T^{-1}]; and the pore size index, φ. The final term of equation (1), the soil moisture uptake function, U, is presented in a later section (equation (25)).

2.2. Modification of the Hillslope Boussinesq Model

[19] The addition into the above model of saturated lateral flow allows for the consideration of heterogeneous potentiometric curvature in the investigation of multiple water table attractors. It also allows for future calibration to distributed observed groundwater levels. A hillslope storage Boussinesq (HSB) equation of one-dimensional lateral flow that accounts for catchment shape and the slope of the impermeable bed was adopted [*Troch et al.*, 2003]. As the catchment geometry (catchment width, slope, and depth to basement) is defined by few model parameters, it also facilitates tractable future investigation into their role in the emergence of multiple attractors.

[20] Application of the HSB model to dryland salinity investigations is likely to misrepresent dryland salinity processes due to its constant bed slope angle. As illustrated by the common example of a shallow water table occurring at the break of slope, topographic curvature heavily influences the depth to water table and cannot be assumed zero for this investigation. *Hilberts et al.* [2004] proposed a nonuniform sloping bed HSB, such that the slope angle, i, is a function of distance to the outlet, x. This expansion and *Troch et al.* [2003] provided the basis on which the following modifications to the HSB were made: a soil layer of porosity differing to the underlying consolidated sediments; recharge as a function of depth to water table; and uptake (deposition) of soil moisture when the water table rises within the soil layer.

[21] *Troch et al.* [2003] modified the saturated lateral flow Boussinesq equation to a hillslope of variable width, $w(x)$, by changing the state variable from saturated thickness, b, to groundwater storage, S:

$$\frac{dS}{dt} = \frac{\partial}{\partial x} \left\{ -\frac{k_s S}{f} \left[\cos i \frac{\partial}{\partial x} \left(\frac{S}{wf} \right) + \sin i \right] \right\} + N \tag{17}$$

where x [L] is the distance to the outlet measured parallel to the impermeable aquifer basement; f is a dimensionless parameter for the drainable porosity; i is the slope of the aquifer basement to the horizontal; k_s [L T^{-1}] is the saturated lateral conductivity; and N is the source term representing net recharge at distance x and time t. It assumes groundwater flow occurs only in the direction x and that the saturated thickness, $\overline{b}$, is uniform over the catchment width at x and is equal to $\frac{S}{wf}$.

[22] Previous applications of this equation assumed the drainable porosity, f, to be either constant [e.g., *Troch et al.*, 2003; *Hilberts et al.*, 2004] or a function of the soil-water retention properties and thus the water table depth [*Hilberts et al.*, 2007]. Neither considered two or more layers of differing saturated porosity. In this application it is too restrictive to assume the soil and underlying unconfined aquifer are of equal saturated porosity. Thus equation (17) is modified such that f is replaced by a bulk drainable porosity, μ, which is a function of the groundwater storage estimated across both layers and derived as follows:

$$\begin{aligned} \overline{b} &= \frac{S}{w\mu} \\ &= \frac{S}{wf} - (S > S_{aq}) \left(\frac{S - S_{aq}}{w\phi} + \frac{S - S_{aq}}{wf} \right) \\ &= \frac{S}{wf} - (S > S_{aq}) (S - S_{aq}) \frac{\phi - f}{\phi f} \end{aligned} \tag{18}$$

where S_{aq} [L^2] is the capacity of groundwater storage below the lower soil boundary (see equation (22)); and f is the drainable porosity of the underlying unconfined aquifer.

The equation effectively calculates the saturated thickness from the groundwater storage, S, assuming both layers have a porosity of f, and subtracts from it the saturated thickness for groundwater storage within the soil layer, calculated using the porosity of both f and ϕ. Rearranging as a function for μ gives:

$$\mu = \frac{Sf}{S - (S > S_{aq})(S - S_{aq})\frac{\phi - f}{\phi f}} \tag{19}$$

[23] The step function ($S > S_{aq}$) equals unity when S is greater than S_{aq} and is otherwise zero. This causes a discontinuity in the model, and so was replaced by a smooth approximation. Importantly, an approximation using equation (16) causes μ to implausibly be less than f as S increases toward S_{aq}. Using the integral of equation (16) with respect to S ensures μ to be greater than f as S increases toward S_{aq}. Thus the bulk drainable porosity is redefined as follows (see *Kavetski and Kuczera* [2007], equations (12)–(13), for further details):

$$\mu = \frac{Sf}{S - \frac{\phi - f}{\phi}\int_0^S \lambda dS} \tag{20}$$

where

$$\int_0^S \lambda dS = \lambda_S \ln\left(e^{\frac{S - S_{aq}}{\lambda_S}} + 1\right) \tag{21}$$

[24] To complete the derivation of μ, the constant vector S_{aq} is defined as follows, where d_{soil} is a dimensionless parameter for the depth of the soil layer as a fraction of the vertical depth from the surface to the aquifer basement. This representation of soil depth facilitates a declining soil depth as the aquifer basement approaches the surface at the upper catchment:

$$S_{aq} = \frac{b_{aq}}{wf} = \frac{1}{wf}(1 - d_{soil})(\overline{E} - \overline{B})\cos i \tag{22}$$

where $\overline{E}$ [L] is the elevation of the land surface at x averaged over the catchment width at x; $\overline{B}$ [L] is the elevation of the impermeable bedrock at x also averaged over the catchment width at x; b_{aq} [L] is the thickness between the aquifer basement and the soil aquifer. In the implementation of the model $\overline{E}$ and $\overline{B}$ were estimated as a function of the horizontal distance from the catchment outlet, u, rather than parallel to the impermeable aquifer basement, x. The term cos i converts the vertical thickness, $\overline{E} - \overline{B}$, to a thickness perpendicular to x.

[25] Two additional aspects of the two-layer version of equation (17) are that, firstly, a rising (falling) water table will remove water from (deposit water to) the unsaturated zone and, secondly, as the water table approaches the surface, groundwater will be evaporated. As the inclusion of groundwater evaporation into the model is only to provide a negative feedback to constrain the water table below the surface, a simple equation is adopted for which no additional parameters are required. From the unsaturated zone evaporation function (equation (12)), the relative evaporative potential decay provides an estimate of groundwater evaporation from the top of the capillary fringe in the form:

$$E_{gw} = PETe^{-a(d_v - \psi_a)} \tag{23}$$

where d_v [L] is the minimum of the vertical depth of the soil layer and the depth to the water table, defined as:

$$d_v = \overline{E} - \overline{B} - \frac{S}{w\mu\cos i} \tag{24}$$

[26] The uptake (deposition) of soil moisture by a rising (declining) water table is poorly represented by a lumped unsaturated zone model. For example, the uptake is a function of the soil moisture at a depth near the initial water table, yet for a lumped model the soil moisture is assumed uniform. Also, hysteresis effects may occur, as the response from a rising and falling water table is unlikely to be equal. More relevant to this study is that, as the soil moisture fraction is estimated from the soil moisture storage, m, divided by d_v, a rising water table will cause, when flux changes are ignored, an increase of the soil moisture fraction. For the scenario of a water table within the soil layer but below the root zone, it is implausible that a rising water table would increase the relative soil moisture, and thus increase transpiration and evaporation, despite no additional soil moisture. The uptake function has thus been developed such that the soil moisture fraction is constant with a changing water table depth and achieved via the uptake of unsaturated storage equaling the soil moisture fraction multiplied by the rate of water table rise. The discontinuity, ($S < S_{aq}$), in the following was removed by substituting equation (16) for λ.

$$\begin{aligned} U &= w\theta\frac{d\overline{b}}{dt} \\ &= w\theta\frac{d}{dt}\left(\frac{S}{w\mu}\right) \\ &= \theta\frac{dS}{dt}\mu^{-1}\left(1 - \frac{S}{\mu}\frac{\partial\mu}{\partial S}\right) \\ &= (S < S_{aq})\frac{\theta}{\phi}\frac{dS}{dt} \\ &= \lambda\frac{\theta}{\phi}\frac{dS}{dt} \end{aligned} \tag{25}$$

[27] Generalizing the HSB of equation (17) such that the bedslope, i, and lateral saturated conductivity, k_s, are not assumed uniform; replacing f with μ; substituting the source term, N, with recharge (equation (14)), groundwater evaporation (equation (23)) and the groundwater uptake (equation (25)); and rearranging to an explicit equation for $\frac{dS}{dt}$ the HSB becomes:

$$\frac{dS}{dt} = \frac{1}{\mu\left(1 - \lambda\frac{\theta}{\phi}\right)}\left\{\frac{\partial}{\partial x}\left[\frac{k_s S}{\mu}\left(\cos i\frac{\partial\overline{b}}{\partial x} + \sin i\right)\right] + w(L - E_{gw})\right\} \tag{26}$$

[28] Importantly, the denominator of the outer term in the above equation causes the rate of change of groundwater

Table 1. Model Parameters and Assigned Values

Catchment Geometry Parameters	
Catchment length, L	2000 m
Elevation of aquifer basement, $B_3u^2 + B_2u + B_1$	$1.75e^{-5}$, 0.003, 0
Elevation of land surface, $E_3u^2 + E_2u + E_1$	$1e^{-5}$, 0, 50
Catchment width, $2w_1e^{w_2u}$	250 m, 0.0004
Soil depth (as fraction of depth to bedrock)	0.05
Hydrogeological Parameters	
Lateral saturated hydraulic conductivity, $k_{s_{\max}}$	1.0 m day^{-1}
Specific yield, f	0.05
Lower boundary condition hydraulic gradient	0.001
Upper boundary condition specified flux	0 m^3 day^{-1}
Unsaturated Zone Parameters	
Limiting infiltration rate, I_0	0.02 m day^{-1}
Brooks and Corey soil parameters, φ, ψ_a	0.168, −0.2917 m
Vertical conductivity, k_v	0.0288 m day^{-1}
Porosity, ϕ	0.43
Residual soil moisture fraction, θ_r	0.109
Evaporation depth at 5% relative potential, d_{evap}	0.5 m
Fraction of potential evaporation at depth d_{evap}, Γ	0.05
Plant Water Use Parameters	
Stomata closure soil moisture, θ_*	0.35
Wilting point soil moisture, θ_{wp}	0.1752
Canopy light extinction coefficient, k_{light}	0.6
Depth at which LAI_t is 50% of potential, $d_{LAI/2}$	2 m
LAI rate of decay with water table depth, α	3
Change In LAI with the rainfall ratio, β	1
Threshold Smoothing Parameters	
Infiltration capacity smoothing, λ_P	0.005 m
Soil moisture fraction smoothing, λ_θ	0.001
Lower soil boundary smoothing, λ_S	40 m^2
Saturated thickness at which $k_s = 0.5k_{s_{\max}}$, $b_{k/2}$	2 m
Rate of decline of k_s with saturated thickness, τ	4

storage to be a function of the soil moisture. For a water table within the soil layer, as the soil moisture approaches saturation $\frac{dS}{dt}$ approaches infinity, thus causing a singularity. While this has not occurred in simulations to date, caution is required in future applications. In solving equation (26) the inner and outer partial derivatives were approximated by block-centered finite difference, such that, at block j:

$$\frac{dS_j}{dt} \approx \frac{1}{\mu_j\left(1-\lambda_j\frac{\theta_j}{\phi}\right)} \cdot \left\{\frac{1}{x_{j+\frac{1}{2}}-x_{j-\frac{1}{2}}}\left[C_{j+\frac{1}{2}}\left(\cos i_{j+\frac{1}{2}}\frac{\overline{b_{j+1}}-\overline{b_j}}{x_{j+1}-x_j}+\sin i_{j+\frac{1}{2}}\right) - C_{j-\frac{1}{2}}\left(\cos i_{j-\frac{1}{2}}\frac{\overline{b_j}-\overline{b_{j-1}}}{x_j-x_{j-1}}+\sin i_{j-\frac{1}{2}}\right)\right] + w_j\left(L_j - E_{gw_j}\right)\right\} \quad (27)$$

where C is the lateral flow conductance and equals $\frac{k_sS}{\mu}$. For an unconfined aquifer and assuming the transmissivity varies linearly between the block nodes, the conductance at $j-\frac{1}{2}$ and $j+\frac{1}{2}$ is approximated as [*Harbaugh et al.*, 2000; *Goode and Appel*, 1992]:

$$C_{j-\frac{1}{2}} = \frac{1}{2}\left(C_j + C_{j-1}\right), \quad C_{j+\frac{1}{2}} = \frac{1}{2}\left(C_{j+1} + C_j\right) \quad (28)$$

[29] The slope of the bedrock, i, is defined as a function of the bedrock slope relative to the horizontal distance to the outlet, u [L], below. In this implementation, $i_{j\pm\frac{1}{2}}$ was estimated by linear interpolation from the adjacent block nodes:

$$i_j = \arctan\frac{\partial\overline{B_j}}{\partial u_j} \quad (29)$$

[30] Saturated conductivity was estimated as a logistic function such that as the saturated thickness approaches zero, k_s rapidly approaches zero. More specifically, at a saturated thickness of $b_{k/2}$ [L] the saturated conductivity is half the maximum, $k_{s_{\max}}$ [L T^{-1}], and declines at a rate τ with the saturated thickness. This was implemented to avoid the requirement for an additional state variable vector, as per ModFlow [*Harbaugh et al.*, 2000], for the rewetting of dry nodes.

$$k_s = k_{s_{\max}}\frac{b^\tau}{b^\tau + b_{k/2}^\tau} \quad (30)$$

2.3. Numerical Solution

[31] An analytical solution to the above nonlinear coupled unsaturated HSB PDE (equations (1) and (27)) is both very unlikely and not the focus of this paper. Numerical solution methods were therefore adopted. They were solved as a transient problem using the MatLab variable time step solver *ode*15*s* [*Shampine and Reichelt*, 1997]; u was discretized at 10 m; and relative and absolute error tolerances were 10^{-4} and 10^{-6} respectively. Validation of the solution involved (1) confirmation of mass balance errors less than 0.1 mm day^{-1} and (2) validation of the mass balance errors being proportional to the spatial node spacing, relative and absolute error.

[32] Limit cycle continuation (LCC) traces stable periodic cycles of the state variables with a change in a model parameter. Unlike time integrated solutions, it allows estimation of the state-space location of repellors in addition to attractors. It was undertaken using MATCONT-CL [*Dhooge et al.*, 2003] with the following modifications: (1) center weighted finite difference Jacobian with adaptive finite difference step size [*Ridders*, 1982] and (2) boundary value problem (BVP) collocation scheme modified for periodicity resulting from forcing (seasonal climate data) and not the differential equations. The continuation was undertaken for the saturated lateral conductivity parameter, $k_{s_{\max}}$. The BVP was solved with seven solution nodes and five collocation points between each node; maximum step length of 1000 (dimensionless); and a normal vector tolerance for the Newton's residual and function error of 10^{-6}. The LCC results were checked at the fold points (i.e., at the $k_{s_{\max}}$ limit of an attractor) against time integration solutions.

3. Model Exploration

[33] In exploring model behavior, parameters typical of a semiarid catchment have been adopted and are presented in Table 1. The land use is grazed pastures and soil-water parameters are for a sandy clay [*Rawls et al.*, 1982]. The repeating within-year climatic forcing and average LAI (LAI_{month}) are presented in Figure 2. The monthly climatic

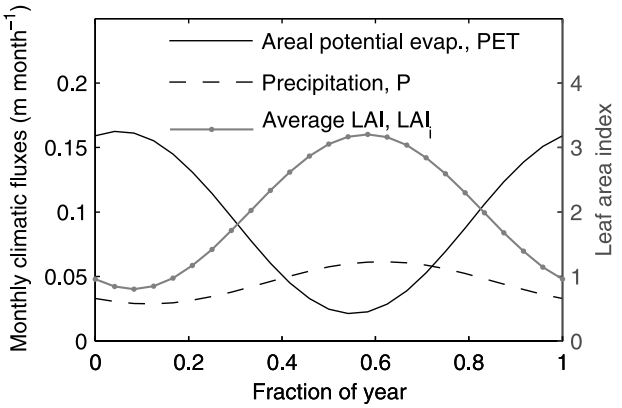

Figure 2. Climatic forcing and average LAI (LAI_{month}).

forcing were converted to the annual scaling of the model prior to implementation.

3.1. Transient Solutions

[34] If a water table has only one attractor, then irrespective of the initial head or magnitude of disturbance it will eventually return to the same attractor. To investigate the potential for two attractors the model was solved with an initial head of 20% and 98% of the maximum saturated thickness. Importantly, it is implausible to expect all dryland catchments to have the same number of attractors. The exploration is thus undertaken at three values of saturated lateral conductivity, $k_{s_{max}}$.

[35] Figures 3, 4, 5, and 6 show simulation results from the two initial heads and, for Figures 3 and 5, at three values of $k_{s_{max}}$. Displayed in each cross section is the initial head; the transient solution at 20 year increments; and the steady state head (at the first day of each year). As a result of the cyclical climatic forcing the head does not approach a steady state at x but rather approaches a stable within-year sinusoidal like cycle. The steady state head was identified by continuing the simulation until the soil moisture and groundwater storage state variables at all nodes of x converged to, and maintained, a stable phase space cycle for at least 100 years simulation. In the following subsections the model is investigated for two types of lower boundary condition: fixed hydraulic gradient and a general head boundary.

3.1.1. Fixed Hydraulic Gradient at $x = 0$ m

[36] In the following, the lower boundary condition is a constant phreatic surface hydraulic gradient of 0.001. This boundary condition, compared to more conventional boundary conditions such as fixed head, fixed flow rate or general head, allows the rate of saturated outflow to be relatively unconstrained. For a low $k_{s_{max}}$ of 0.075 m day^{-1} and the shallow initial head, Figure 3a shows a very slight rise of the water table to 0.68 m DBNS (at 250 m from the outlet and henceforth). From the deep initial head, Figure 3b shows a significant rise of the water table to an elevation equal to that from the shallow initial condition (Figure 3a). Therefore at a $k_{s_{max}}$ of 0.075 m day^{-1} the model has only one steady state water table depth and thus one attractor. For a $k_{s_{max}}$ of 1.0 m day^{-1} and the shallow initial head, Figure 3c shows a convergence to a shallow water table of 0.9 m DBNS. Conversely, from the deep initial head Figure 3d shows an initial rise and eventual convergence to a deep water table of 45.7 m DBNS. Therefore at a $k_{s_{max}}$ of 1.0 m day^{-1} the model has two steady state water table depths and thus two attractors. For a higher $k_{s_{max}}$ of 2.5 m day^{-1}, Figures 3e–3f show that from the shallow and deep initial heads, both solutions converge to an equal DBNS over the catchment extent and equaling 47.4 m DBNS at 250 m from the outlet. Therefore at a $k_{s_{max}}$ of 2.5 m day^{-1} the lateral discharge at the lower boundary is sufficient that the shallow attractor is eliminated and the model has only one attractor.

[37] To provide a comparison with more traditional groundwater models, and to make transparent the process causing the two attractors, the LAI (equation (7)) is made independent of the water table depth via removal of the equations logistic function. This is the only change in the model, data or parameters from the model producing the results of Figure 3. Figures 4a and 4b show simulation results for a $k_{s_{max}}$ of 1.0 m day^{-1} from both the shallow and deep initial head. Both converge to the same attractor of 45.7 m DBNS, which is identical to the deep DBNS attractor of Figure 3d for $k_{s_{max}}$ of 1.0 m day^{-1}. The inclusion into the model of LAI as a function of DBNS produces a positive feedback such that when the water table is shallow a net recharge event causes an elevation of the water table, which reduces LAI, and thus transpiration. During subsequent recharge events, less infiltrated water is transpired resulting in a higher soil moisture fraction and recharge than would occur if the LAI were independent of the water table depth. The increased recharge further elevates the water table, causes a further reduction in the LAI, and results in the shallow attractor of Figure 3c.

3.1.2. General Head Boundary at $x = 0$ m

[38] The above exploration clearly highlights the emergence of multiple water table attractors. The fixed hydraulic gradient lower boundary condition is, however, uncommon. In the following it has been replaced with a general head (GH) boundary, simulating the interaction with a river perpendicular to the groundwater flow. The GH boundary is implemented as a river of fixed water level elevation, extending over the width of the catchment and at $x = 0$ m:

$$Q_{x=0} = k_{riv} w \, h_{riv} \frac{h_{x=0} - h_{riv}}{d_{riv}} \tag{31}$$

$$= C_{riv} w (h_{x=0} - h_{riv}) \tag{32}$$

where $h_{x=0}$ is the vertical water table elevation at $x = 0$ m equaling $\overline{B} + \frac{b}{\cos i}$; h_{riv} [L] is a parameter for the elevation of the river water level; and C_{riv} [L T^{-1}] a parameter for the river conductance per unit boundary width. The latter lumps the parameters of $\frac{k_{riv} b_{riv}}{d_{riv}}$, where k_{riv} [L T^{-1}] is the lateral saturated conductivity between the river and groundwater; b_{riv} [L] is the depth of saturated flow into the river; and d_{riv} [L] is the distance between the $x = 0$ m model node and the river. The parameters h_{riv} and C_{stream} were set to 48 m and 0.2 m day^{-1} respectively.

[39] Figure 5 shows simulation results from the two initial heads and three values of $k_{s_{max}}$. For a low $k_{s_{max}}$ of 0.1 m day^{-1}, solutions from both the shallow and deep initial heads converge to 0.68 m DBNS (Figures 5a and 5b). Therefore at a $k_{s_{max}}$ of 0.1 m day^{-1} the model has only one steady state water table depth and thus one attractor. For a

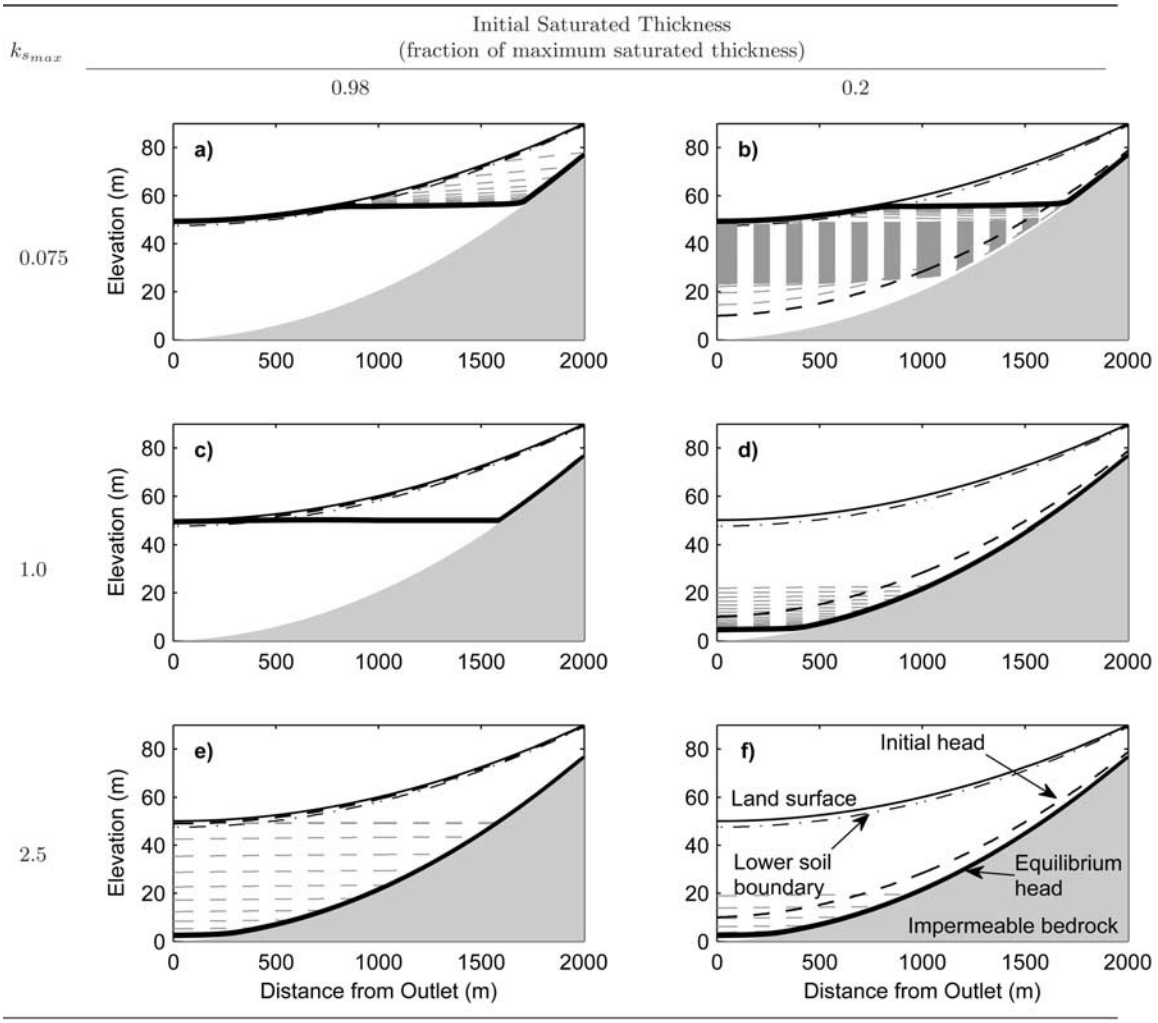

Figure 3. Time integration solutions of the model at two initial heads (as a fraction of the maximum saturated thickness $\frac{b}{b_{\max}}$) for three values of saturated lateral conductivity $k_{s_{\max}}$. On each cross section (labeled in the bottom right) is the land surface elevation, basement elevation, and initial and steady state groundwater heads. Transient solutions at 20-year time steps are given as light gray lines.

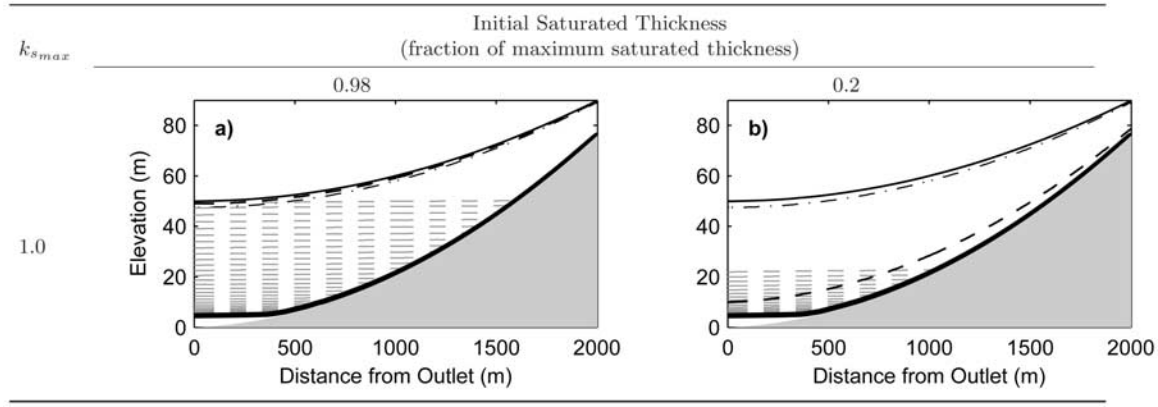

Figure 4. Time integration solutions of the model without the positive feedback at two initial heads (as a fraction of the maximum saturated thickness $\frac{b}{b_{\max}}$) at a saturated lateral conductivity $k_{s_{\max}}$ of 1.0 m day^{-1}. On each cross section is the land surface elevation, basement elevation, and initial and steady state groundwater heads. Transient solutions at 20-year time steps are given as light gray lines.

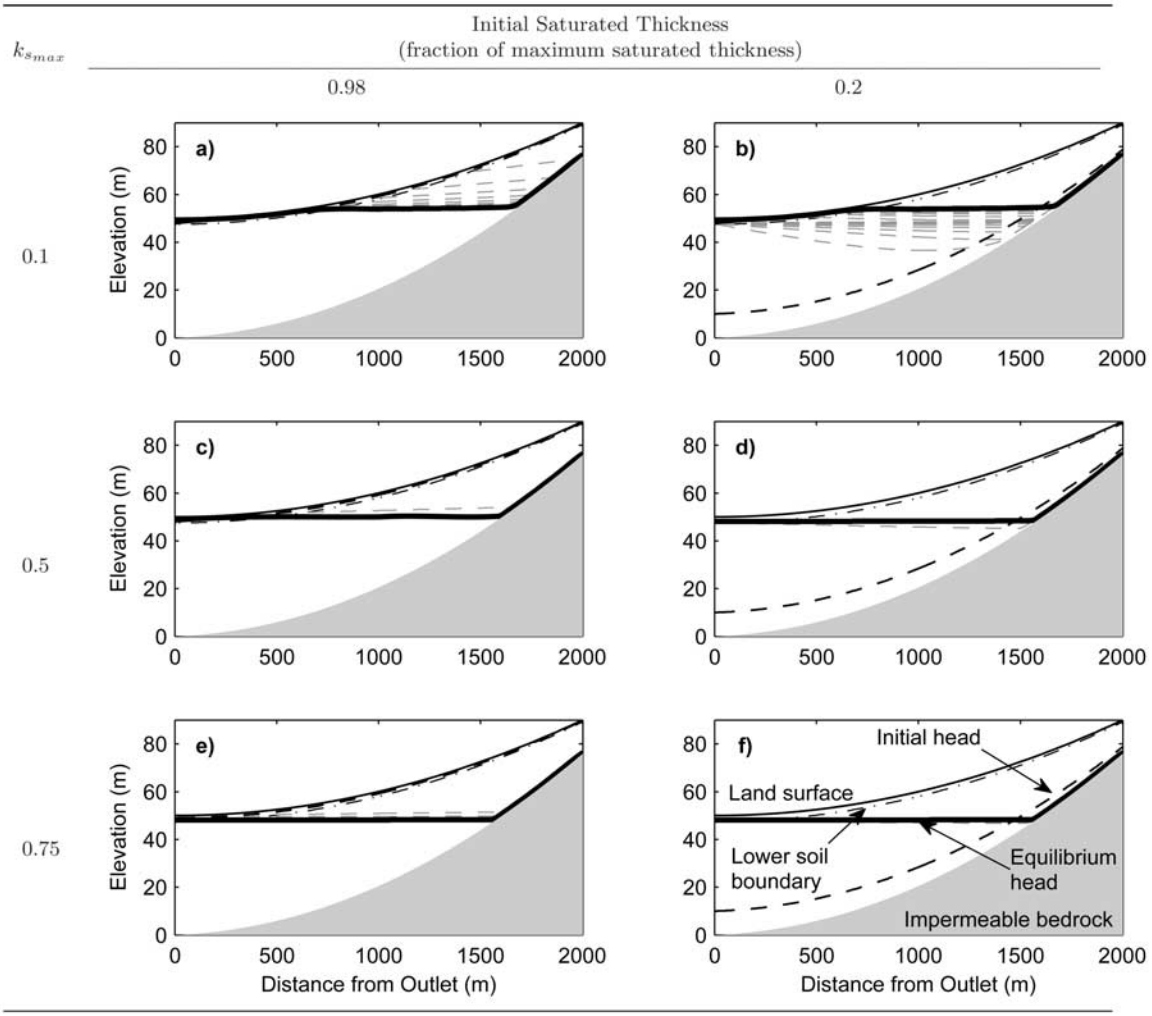

Figure 5. Time integration solutions of the GH boundary condition model at two initial heads (as a fraction of the maximum saturated thickness $\frac{b}{b_{\max}}$) for three values of saturated lateral conductivity $k_{s_{\max}}$. On each cross section (labeled in the bottom right) is the land surface elevation, basement elevation, and initial and steady state groundwater heads. Transient solutions at 20-year time steps are given as light gray lines.

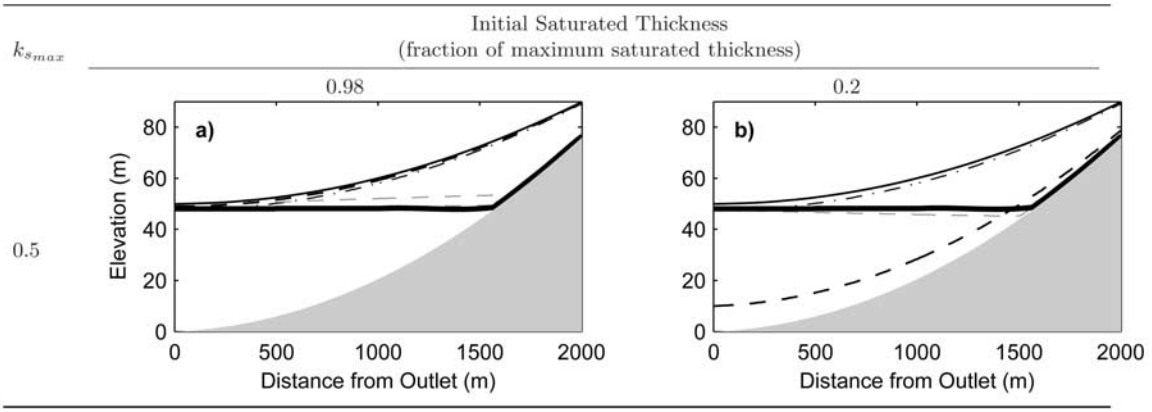

Figure 6. Time integration solutions of the GH boundary condition model without the positive feedback at two initial heads (as a fraction of the maximum saturated thickness $\frac{b}{b_{\max}}$) at a saturated lateral conductivity $k_{s_{\max}}$ of 0.5 m day^{-1}. On each cross section is the land surface elevation, basement elevation, and initial and steady state groundwater heads. Transient solutions at 20-year time steps are given as light gray lines.

higher $k_{s_{max}}$ of 0.5 m day^{-1}, from the shallow and deep initial heads the solutions converge to 0.9 and 2.51 m DBNS respectively (Figures 5c and 5d). While this difference is subtle and apparent only at $u \leq 750$ m, at a $k_{s_{max}}$ of 0.5 m day^{-1} the model does have two attractors. For a higher $k_{s_{max}}$ of 0.75 m day^{-1}, solutions from both the shallow and deep initial heads converge to 2.53 m DBNS (Figures 5e and 5f). Therefore at a $k_{s_{max}}$ of 0.75 m day^{-1} the model also has only the deep attractor.

[40] Again, a comparison was undertaken with more traditional groundwater models by removing the logistic term of the LAI equation (equation (7)). Figures 6a and 6b show simulation results for a $k_{s_{max}}$ of 0.5 m day^{-1} from both the shallow and deep initial head. Both converge to the same attractor of 2.56 m DBNS. Again, the inclusion of LAI as a function of DBNS produces a positive feedback resulting in two attractors. For the prior boundary condition (section 3.1.1) the simulations with and without the LAI dependency resulted in a deep attractor of equal water table depth. For the GH boundary, though, the water table is three centimeters shallower when the LAI dependency is included because at a depth of 2.53 m (Figure 5c) the LAI is still slightly constrained and recharge is slightly increased.

3.2. Forced Limit Cycle Continuation

[41] Figures 3 and 5 illustrate that two attractors emerge only within a specific range of $k_{s_{max}}$. The significance of these multiple attractors is though dependent upon the size of the $k_{s_{max}}$ range. That is, if two attractors emerge over a wide range of $k_{s_{max}}$ then a larger fraction of a region's catchments may have two attractors. Also, if the state-space distance from the current attractor to a repellor is very large then the probability of a disturbance being of sufficient magnitude to cause a shift over the repellor is minimal, making the alternate attractor of minimal significance. Continuation analysis (a subset of bifurcation theory) is a powerful tool for (1) quantifying the state-space location of attractors and repellors with a change in one or two model parameters and (2) quantifying the hysteresis in recovery following a change in the basin of attraction when the model parameter(s) investigated are management initiatives, such as the fraction of a landscape cleared. Below, results of numerical continuation analysis quantify (1) the $k_{s_{max}}$ range over which two attractors occur and (2) the state-space location of repellors within this $k_{s_{max}}$ region.

[42] Prior to considering limit cycle continuation (LCC), consider a system without any periodicity in the attractor. For example, if in the above model the climate and monthly average LAI were constant for all time, then the solution would converge to a constant over time. Equilibrium continuation is the process of tracing such a solution with a change in a model parameter. That is, for a scalar state variable problem, y, with parameter a, equilibrium continuation traces $\frac{dy}{dt} = g(y, a) = 0$ from an initial solution with a change in parameter a. For trivial problems the solution is obtained by rearranging $\frac{dy}{dt}$ to an explicit function for a, that is, $a = g(y)$. For implicit equations a predictor-Newtons corrector method is used to numerically trace a curve from an initial solution. The stability of each point is defined by the eigenvalues such that if all eigenvalues are negative (real or complex) the point is an attractor while if at least one eigenvalue is greater than zero the point is a repellor. The significance of such a curve is that, in this paper's context, it quantifies the parameter region over which only a single attractor exists, the region over which multiple attractors exist, and the state variable location of the repellor(s). Quantifying the state-space distance from an attractor to a threshold is a common measure of resilience [*Lele*, 1998]. This effectively estimates the cumulative disturbance required to cross the threshold, without any requirement to quantify the sequence, frequency or magnitude of the disturbances.

[43] As a result of the model within-year periodic forcing, the soil moisture and groundwater storage state variables do not approach a time-independent equilibrium but rather a sinusoidal-like repeating cycle, formally called a limit cycle. As the cycle results from climatic forcing rather than the system equations, it is referred to henceforth as a *forced* limit cycle. Limit cycle continuation effectively traces a phase plane with incremental changes in a parameter. It was undertaken by treating the cycle of the state variables as a boundary value problem (BVP), and solved using a collocation algorithm. As per equilibrium continuation, limit cycle continuation starts from an initial limit cycle derived from time integration of the model and, using a predictor-corrector algorithm, increments the model parameter of interest and attempts convergence of the BVP. As per section 3.1, the investigation was undertaken for the parameter $k_{s_{max}}$ and for both the fixed hydraulic gradient and general head boundary conditions. Forced limit cycle continuation results are presented at two cross-section locations (250 and 1000 m) in two and three dimensions.

3.2.1. Fixed Hydraulic Gradient at $x = 0$ m

[44] Figure 7 presents the LCC results at two cross-section locations with the inclusion of the LAI dependency (a and b) and with its omission (c and d). Each line (actually a phase cycle) parallel to the soil moisture axis is a solution to the BVP. The line approximately parallel to the $k_{s_{max}}$ axis identifies the solution path and starts from the initial solution (dotted) at a $k_{s_{max}}$ of 2.5 m day^{-1}. In all following plots, a dashed solution path identifies a model repellor and a solid line identifies an attractor. In Figures 7e and 7f, the solution paths (lower soil moisture path only) from each of the three-dimensional models are overlain and, for clear comparison, rotated to omit the soil moisture variable and to clearly display the differences in water table depth.

[45] Figures 7a and 7b illustrate that at both 250 and 1000 m, two attractors occur between a $k_{s_{max}}$ of 0.1 and 2.4 m day^{-1}. In this region the attractor to which a time integration solution of the model will converge, assuming the climatic forcing of Figure 2, depends upon the initial conditions. That is, it will converge to the attractor for which crossing of the repellor is not required. The repellor could though be crossed if a climatic disturbance was sufficient to move the state variables over the repellor. The resilience of each attractor is thus the state variable distance from the attractor to the repellor [*Lele*, 1998]. Between a $k_{s_{max}}$ of 0.1 and 2.4 m day^{-1} the model thus has a finite resilience to climatic disturbances. Below a $k_{s_{max}}$ of 0.1 m day^{-1} the time integration solution of the model will converge only to the shallow attractor, independent of the initial conditions. Conversely, above 2.4 m day^{-1} the time integration solution will converge only to the deep attractor, independent of the initial conditions. Both single-attractor regions are thus of an infinite resilience to climatic disturbances. For a diagram-

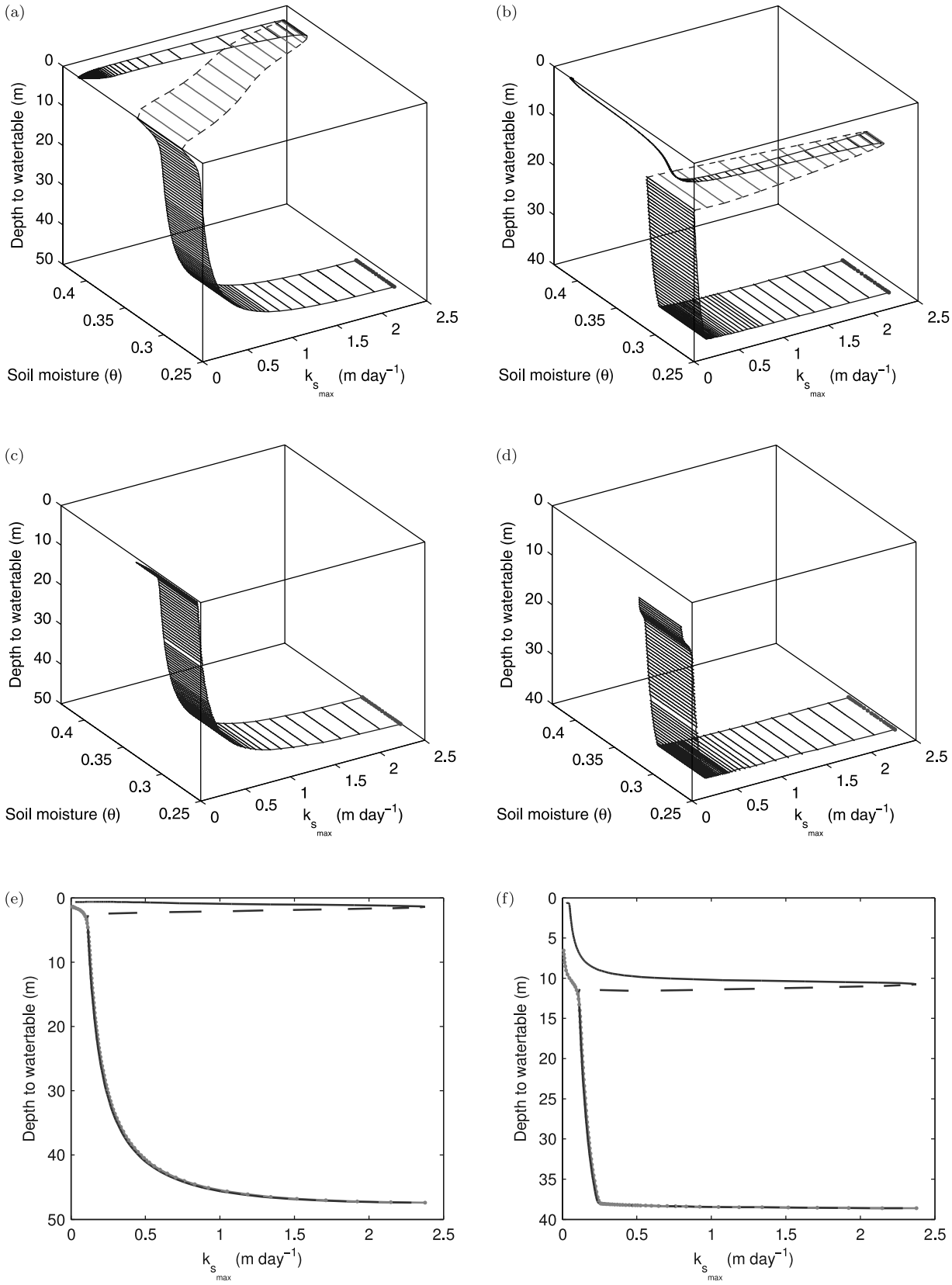

Figure 7. Fixed hydraulic gradient lower boundary condition forced limit cycle continuation results at two distances from the catchment outlet. Solid lines identify attractors, and dashed lines identify repellors. (a) 250 m. (b) 1000 m. (c) 250 m, no positive feedback. (d) 1000 m, no positive feedback. (e) 250 m (two-dimensional)-feedback model (solid black) and no positive feedback model (gray dotted). (f) 1000 m (two-dimensional)-feedback model (solid black) and no positive feedback model (gray dotted).

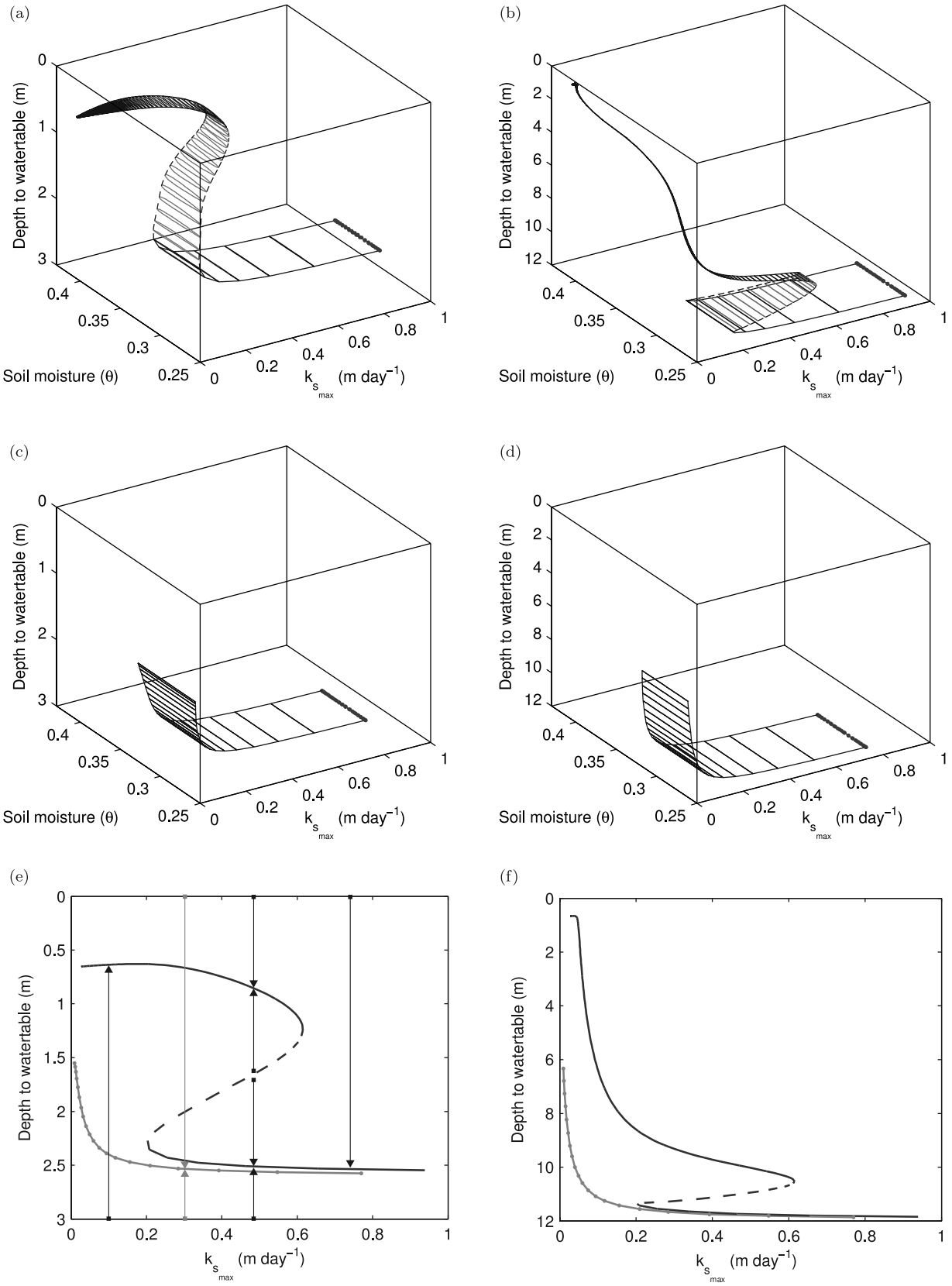
(a)
Depth to watertable (m)
Soil moisture (θ)
$k_{s_{max}}$ (m day^{-1})
(b)
Depth to watertable (m)
Soil moisture (θ)
$k_{s_{max}}$ (m day^{-1})
(c)
Depth to watertable (m)
Soil moisture (θ)
$k_{s_{max}}$ (m day^{-1})
(d)
Depth to watertable (m)
Soil moisture (θ)
$k_{s_{max}}$ (m day^{-1})
(e)
Depth to watertable (m)
$k_{s_{max}}$ (m day^{-1})
(f)
Depth to watertable (m)
$k_{s_{max}}$ (m day^{-1})

Figure 8

matic illustration of these concepts, see Figure 8e. With respect to the range of each limit cycle, the most significant aspect is the reduced soil moisture variability of the shallow attractor compared to the deep attractor.

[46] To further highlight the influence of the positive feedback from LAI declining with the water table depth, equation (7) is again made independent of the water table depth via removal of the logistic function. In Figures 7c and 7d are the LCC results at 250 and 1000 m. At all values of $k_{s_{max}}$ this model has only one attractor and no repellor and thus is infinitely resilient to climatic disturbances.

[47] Figures 7e and 7f provide a comparison of the LCC results from the model for which the LAI is dependent and independent of the water table depth. At both locations the two models differ significantly only at a water table depth shallower than the repellor, below which the models are approximately equal. The shallow attractor of the water table-dependent model emerges at a relatively shallow depth and is also less resilient than the deeper attractor.

3.2.2. General Head Boundary at $x = 0$ m

[48] Figure 8 presents the LCC results at two cross section locations with the inclusion of the LAI dependency (a and b), and with its omission (c and d). Figures 8a and 8b illustrate that at both 250 and 1000 m, two attractors occur between a $k_{s_{max}}$ of 0.2 and 0.61 m day^{-1}. Below a $k_{s_{max}}$ of 0.2 m day^{-1} the time integration solution of the model will converge only to the shallow attractor, independent of the initial conditions. Conversely, above 0.61 m day^{-1} the time integration solution will converge only to the deep attractor, again independent of the initial conditions. Both single-attractor regions are thus of an infinite resilience to climatic disturbances. With respect to the range of each limit cycle, the most significant aspect, similar to the prior boundary condition, is the reduced soil moisture variability of the shallow attractor compared to the deep attractor.

[49] To again highlight the influence of the positive feedback, equation (7) is made independent of the water table depth via removal of the logistic function. Figures 8c and 8d show the LCC results at 250 and 1000 m. At all values of $k_{s_{max}}$ this model has only one attractor and no repellor and is thus infinitely resilient to climatic disturbances.

[50] Figures 8e and 8f provide a comparison of the LCC results from the model for which the LAI is dependent, and independent, of water table depth. The two models differ significantly at both locations and over much of the range of $k_{s_{max}}$. This arises because, for the GH boundary, the deep attractor is sufficiently shallow that the LAI reduces from its potential, and thus recharge increases. Within the region of two attractors ($k_{s_{max}}$ range, 0.2–0.61 m day^{-1}) the resilience of each attractor is also comparable.

[51] The significance to water resource management of multiple water table and soil moisture attractors extends beyond changes to groundwater storage and vegetation dynamics. As the GH boundary simulates saturated flow to and from a river at the lower boundary, multiple attractors in streamflow are also possible. To assess this, the runoff R [L T^{-1}] at node u and time t, annual volumetric runoff Q_{runoff} [L^3 T^{-1}], annual base flow $Q_{\text{base flow}}$ [L^3 T^{-1}], and total annual volumetric contribution to the river Q_{riv} [L^3 T^{-1}] were calculated as below, where the integrals were approximated via Simpson's trapezoidal integration:

$$R(u,t) = P_{eff} - I \tag{33}$$

$$Q_{runoff} = \int_0^{t=1} \int_0^{u=L} w(u)R(u,t)du\ dt \tag{34}$$

$$\begin{aligned} Q_{baseflow} &= \int_0^{t=1} C_{riv} w_{u=0}(h_{u=0}(t) - h_{riv})dt \\ &= \int_0^{t=1} 0.2 \times 500(h_{u=0}(t) - 48)dt \end{aligned} \tag{35}$$

$$Q_{riv} = Q_{runoff} + Q_{baseflow} \tag{36}$$

[52] Figure 9 presents the resulting unit area annual base flow and total flow to the river against $k_{s_{max}}$. Two attractors for base flow and total flow exist between a $k_{s_{max}}$ of 0.2 and 0.61 m day^{-1}. This range is identical to that of the state variables in Figure 8. For a $k_{s_{max}}$ of 0.5 m day^{-1} the base flow at the shallow and deep attractor is 0.018 and 0.0012 m year^{-1}, respectively, and the total streamflow is 0.046 and 0.013 m year^{-1}, respectively. As Figures 8e and 8f illustrate, the resilience of each attractor is only 1–2 m of water table elevation, so a change of attractors seems possible and, as such, a significant change in streamflow is plausible.

4. Discussion and Conclusion

[53] This investigation has demonstrated that a simple and plausible coupled vadose-groundwater model can have two qualitatively different water table attractors, making the steady state water table elevation dependent on the initial conditions. The two attractors result from a positive feedback of LAI, and thus transpiration, declining as a recharge event elevates a shallow saline water table, resulting in increased recharge during subsequent recharge events. It was demonstrated that removal of this feedback resulted in only one attractor, such that the steady state water table became independent of the initial conditions. This independence of the steady state to initial conditions is typical of the vast majority of hydrological models.

[54] Not all catchments are thought to have multiple attractors. Their emergence is dependent upon factors controlling lateral saturated flow (hydrogeology, boundary conditions, catchment shape) and recharge. The range in saturated conductivity, $k_{s_{max}}$, over which the two attractors emerge was investigated, via limit cycle continuation and

Figure 8. General Head lower boundary condition forced limit cycle continuation results at two distances from the catchment outlet. Solid lines identify attractors, and dashed lines identify repellors. (a) 250 m. (b) 1000 m. (c) 250 m, no positive feedback. (d) 1000 m, no positive feedback. (e) 250 m (two-dimensional)-feedback model (solid black) and no positive feedback model (gray dotted). The convergence to each attractor from various initial conditions (solid squares) is illustrated for the feedback model (black arrows) at three values of $k_{s_{max}}$ and the no positive feedback model (gray arrows). (f) 1000 m (two-dimensional)-feedback model (solid black) and no positive feedback model (gray dotted).

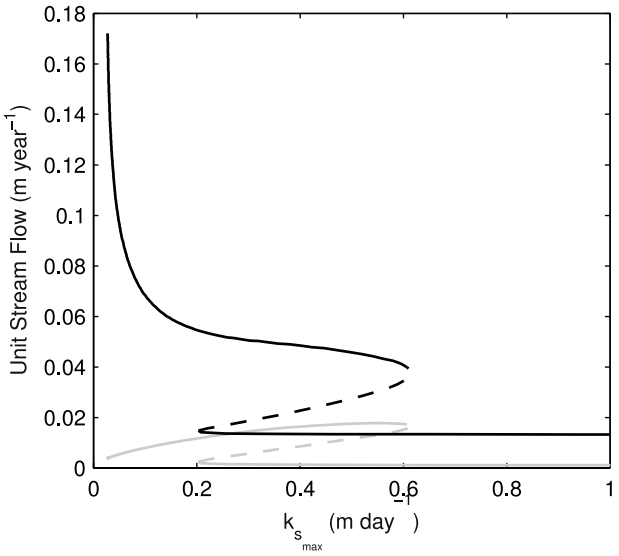

Figure 9. General head lower boundary condition annual base flow (black line) and total streamflow (gray line) at the lower catchment boundary derived from the forced limit cycle continuation. Solid lines identify attractors, and dashed lines identify repellors.

time integration, and found to be 0.1 to 2.4 m day^{-1} for the fixed hydraulic gradient lower-boundary condition and 0.2 to 0.61 m day^{-1} for the general head (GH) lower-boundary condition. Either side of this range only one attractor existed. The difference in range, which was a result of greater lateral flow from the general head boundary condition model, highlights the dependency of this parameter range on model configuration. In earlier trials, for example, doubling the soil layer thickness shifted this range such that two attractor were maintained as $k_{s_{max}}$ approached zero. The most significant differences between the two boundary condition models was the state-space location of the repellor and deep attractor. For the fixed hydraulic gradient condition the repellor water table depth was over 30 m above the deep attractor (Figures 7e and 7f), making it very resilient and suggesting that only the most major of climatic disturbances could cause a change of state from the deep to shallow attractor. For the GH condition, the repellor is approximately centered and is only meters of water table depth from each attractor (Figures 8e and 8f). Climatic disturbances shifting the system to the alternate attractor are thus significantly more plausible for the general head than the hydraulic gradient boundary condition model. Importantly, an attractor change in the general head model, which simulates interaction with a river, would result in major changes to stream water quality and quantity. The catchment contributions of base flow and total river flow both have two attractors, and a change from the shallow to deep attractor would result in a reduction to base flow and total flow of 93% and 71% respectively (Figure 9 at $k_{s_{max}}$ equals 0.5 m day^{-1}).

[55] While the above conclusions are interesting, the unsaturated zone model and its coupling to the lateral flow model is very simple. The omission of explicit salt dynamics required the assumptions that salt fluxes are in pseudoequilibrium, and that the impacts of salt on LAI are immediate. While the sensitivity of vegetation to salt is simulated via two parameters (Table 1, $d_{LAI/2}$ and α), the rate of salt flushing and its correlation with soil type is ignored. The use of monthly climatic forcing data, as opposed to daily, results in a poor estimate of runoff, dampened within-month soil moisture fraction and thus, due to the very nonlinear unsaturated vertical conductivity, reduced recharge. To identify the repellors does though require constant or repeating smooth cyclical climate data. Constant climate data (i.e., annual averages) was investigated and found, as a result of reduced recharge, to significantly reduce both the $k_{s_{max}}$ range and lower value of two attractors compared to monthly data. While the limit cycle continuation results are more valid than those derived from equilibrium continuation, this highlights that the continuation results are dependent upon the time step of the forcing data. That is, if weekly forcing data was used as opposed to the monthly forcing data, the soil moisture would be less smooth, episodic recharge would increase, and estimation of the location and extent over which two attractors occur would be further improved. Despite the above, the model could have been further simplified, for example, by replacement of the partitioning of rainfall to infiltration by a fixed fraction of rainfall; or replacement of matric potential soil-water drainage by a simple function of soil moisture. Both such changes would reduce the number of model parameters but would require additional assumptions. Considering the aims of the investigation, the model is felt sufficiently complex to challenge the assumption of hydrological systems having only one attractor, though simple enough to facilitate identification of repellors, via limit cycle continuation, and future calibration in field studies.

[56] A possible criticism of the findings is that, if catchments have multiple attractors, why have they not been observed? To observe a change from one attractor to another and to attribute this to there being two attractors would require long-term groundwater head monitoring of a catchment that has not undergone notable landuse change; is of a configuration likely to have two attractors; and to have experienced a climatic disturbance sufficient to cause a change of attractors. Unfortunately this is very unlikely and understanding will therefore foreseeably rely on plausible numerical models. However, the potential consequences of assuming a catchment has only one attractor when it actually has two, needs discussion. At the local scale, dryland salinity mitigation could be enhanced via identification of catchments with two attractors and temporary interventions undertaken to shift the water table over the repellor to the deep water table attractor. Assuming all catchments have a single attractor instead requires permanent, and thus more costly, interventions. At the wider scale, and more topical, the water resource impacts from climate change may be significantly amplified for catchments having two attractors. For a catchment currently at the shallow attractor, more extended periods of reduced infiltration may increase the probability of a shift to the deep attractor. Upon such a shift, Figure 9 illustrates catchment yields would dramatically reduce and, importantly, be unlikely to recover following a return to *average* climate conditions. If one attractor instead existed, changes would likely be more proportional to the climatic change and thus less significant. While somewhat alarmist, this highlights the potential changes in natural resource outcomes of

assuming two attractors as opposed to one.

[57] The presented positive feedback is unlikely to be the only positive biophysical feedback in catchment hydrology. Considering that multiple attractors may emerge without positive feedbacks [*Cinquin and Demongeot*, 2002], hydrological systems are even less likely to always have a single attractor. Specifying when and which aspect of a modeled system is assumed to have a single attractor is considered a worthy first step in identifying where other multiple hydrological attractors may exist.

[58] **Acknowledgments.** The authors are grateful for the support received from Australian Research Council grant LP04555338, Murray-Darling Basin Commission, and South Australia Department of Water, Land, and Biodiversity Conservation. The authors also thank Professor John P. Norton of Australian National University for obtaining the above grant and his flexibility in the research direction.

References

Allison, H. E. (2003), Linked social-ecological systems: A case study of the resilience of the western Australian agricultural region, Ph.D. thesis, Murdoch Univ., Perth, WA, Australia.

Allison, H. E., and R. J. Hobbs (2004), Resilience, adaptive capacity, and the lock-in trap of the western Australian agricultural region, *Ecol. Soc.*, *9*(1), 3.

Anderies, J. M. (2005), Minimal models and agroecological policy at the regional scale: An application to salinity problems in southeastern Australia, *Reg. Environ. Change*, *5*(1), 1–17.

Anderies, J., P. Ryan, and B. Walker (2006), Loss of resilience, crisis, and institutional change: Lessons from an intensive agricultural system in southeastern Australia, *Ecosystems*, *9*(6), 865–878.

Argent, R. M., R. J. George, and W. Dawes (2001), Flowtube: A groundwater calculator for salinity estimation, in *MODSIM 2001 International Congress on Modelling and Simulation: Canberra*, edited by F. Ghassemi et al., pp. 621–626, Modelling and Simulation Society of Australia and New Zealand, Canberra, Aust.

Barlow, P., and A. Harbaugh (2006), USGS directions in MODFLOW development, *Groundwater*, *6*(44), 771–774.

Benyon, R., N. Marcar, D. Crawford, and A. Nicholson (1999), Growth and water use of *Eucalyptus camaldulensis* and *E. occidentalis* on a saline discharge site near Wellington, NSW, Australia, *Agric. Water Manage.*, *39*(2–3), 229–244.

Beven, K. J., and M. J. Kirkby (1979), A physically based, variable contributing area model of basin hydrology, *Hydrol. Sci. Bull.*, *24*(1), 43–69.

Beverly, C. R., R. J. Nathan, K. W. J. Malafant, and D. P. Fordham (1999), Development of a simplified unsaturated module for providing recharge estimates to saturated groundwater models, *Hydrol. Processes*, *13*(5), 653–675.

Charney, J., and P. H. Stone (1974), Drought in the Sahara - a biogeophysical feedback mechanism, *Science*, *187*(4175), 434–435.

Chiew, F. H. S., M. C. Peel, and A. W. Western (2002), Application and testing of the simple rainfall-runoff model SIMHYD, in *Mathematical Models of Small Watershed Hydrology and Applications*, edited by V. P. Singh and D. K. Frevert, Water Resources Publications, Littleton, Colo.

Cinquin, O., and J. Demongeot (2002), Roles of positive and negative feedback in biological systems, *C.-R. Biol.*, *325*(11), 1085–1095.

Cordano, E., and R. Rigon (2008), A perturbative view on the subsurface water pressure response at hillslope scale, *Water Resour. Res.*, *44*, W05407, doi:10.1029/2006WR005740.

Dent, C., G. Cumming, and S. Carpenter (2002), Multiple states in river and lake ecosystems, *Philos. Trans. R. Soc. Ser. B*, *357*(1421), 635–645.

Dhooge, A., W. Govaerts, and Y. Kuznetsov (2003), MATCONT: A MATLAB package for numerical bifurcation analysis of ODEs, *ACM Trans. Math. Software*, *29*(2), 141–164.

Dickinson, R., A. Hendersonsellers, C. Rosenzweig, and P. Sellers (1991), Evapotranspiration models with canopy resistance for use in climate models - a review, *Agric. For. Meteorol.*, *54*(2–4), 373–388.

D'Odorico, P., and A. Porporato (2004), Preferential states in soil moisture and climate dynamics, *Proc. Natl. Acad. Sci. U. S. A.*, *101*(24), 8848–8851.

D'Odorico, P., F. Laio, and L. Ridolfi (2005), Noise-induced stability in dryland plant ecosystems, *Proc. Natl. Acad. Sci. U. S. A.*, *102*(31), 10,819–10,822.

Freeze, R. A. (1971), Three-dimensional, transient, saturated-unsaturated flow in a groundwater basin, *Water Resour. Res.*, *7*(2), 347–366.

George, R., R. Nulsen, R. Ferdowsian, and G. Raper (1999), Interactions between trees and groundwaters in recharge and discharge areas - a survey of Western Australian sites, *Agric. Water Manage.*, *39*(2–3), 91–113.

Goode, D. J., and C. A. Appel (1992), Finite-difference interblock transmissivity for unconfined aquifers and for aquifers having smoothly varying transmissivity, *Tech. Rep. 92-4124*, 79 pp., U.S. Geol. Surv., Calif.

Harbaugh, A. W., E. R. Banta, M. C. Hill, and M. G. McDonald (2000), MODFLOW-2000, the U. S. Geological Survey modular ground-water model-user guide to modularization concepts and the ground-water flow process, *Tech. Rep. 00-92*, 121 pp., U.S. Geol. Surv., Reston, Va.

Hilberts, A., E. van Loon, P. Troch, and C. Paniconi (2004), The hillslope-storage Boussinesq model for non-constant bedrock slope, *J. Hydrol.*, *291*(3–4), 160–173.

Hilberts, A., P. Troch, C. Paniconi, and J. Boll (2007), Low-dimensional modeling of hillslope subsurface flow: Relationship between rainfall, recharge, and unsaturated storage dynamics, *Water Resour. Res.*, *43*, W03445, doi:10.1029/2006WR004964.

Holland, K., S. Tyerman, L. Mensforth, and G. Walker (2006), Tree water sources over shallow, saline groundwater in the lower River Murray, south-eastern Australia: Implications for groundwater recharge mechanisms, *Aust. J. Bot.*, *54*(2), 193–205.

Holling, C. S. (1973), Resilience and stability of ecological systems, *Annu. Rev. Ecol. Syst.*, *4*, 1–23, doi:10.1146/annurev.es.04.110173.000245.

Kavetski, D., and G. Kuczera (2007), Model smoothing strategies to remove microscale discontinuities and spurious secondary optima in objective functions in hydrological calibration, *Water Resour. Res.*, *43*, W03411, doi:10.1029/2006WR005195.

Kim, C., G. Salvucci, and D. Entekhabi (1999), Groundwater-surface water interaction and the climatic spatial patterns of hillslope hydrological response, *Hydrol. Earth Syst. Sci.*, *3*(3), 375–384.

Laio, F., A. Porporato, L. Ridolfi, and I. Rodriguez-Iturbe (2001), Plants in water-controlled ecosystems: Active role in hydrologic processes and response to water stress: II. Probabilistic soil moisture dynamics, *Adv. Water Resour.*, *24*(7), 707–723.

Lele, S. (1998), Resilience, sustainability environmentalism, *Environ. Dev. Econ.*, *2*, 221–262.

Ludwig, D., B. Walker, and C. S. Holling (1997), Sustainability, stability, and resilience, *Conserv. Ecol.*, *1*(1), 7.

Monsi, M., and T. Saeki (2005), On the factor light in plant communities and importance for matter production, *Ann. Bot.*, *95*(3), 549–567, doi:10.1093/aob/mci052.

Niswonger, R. G., D. E. Prudic, and R. S. Regan (2006), Documentation of the Unsaturated-Zone Flow (UZF1) package for modeling unsaturated flow between the land surface and the water table with MODFLOW-2005, *Tech. Rep. 6-A19*, 62 pp., U.S. Geol. Surv., Reston, Va.

Peterson, T. J., R. M. Argent, and F. H. S. Chiew (2005), Multiple stable states and thresholds within the goulburn catchment, in *MODSIM 2005 International Congress on Modelling and Simulation*, edited by A. Zerger and R. M. Argent, pp. 2526–2532, Modelling and Simulation Society of Australia and New Zealand, Canberra, Aust.

Rawls, W., D. Brakensiek, and K. Saxton (1982), Estimation of soil-water properties, *Trans. ASAE*, *25*(5), 1316–1328.

Ridders, C. (1982), Accurate computation of f′(x) and f′(x) f″(x), *Adv. Eng. Software*, *4*(2), 75–76.

Ridolfi, L., P. D'Odorico, and F. Laio (2006), Effect of vegetation-water table feedbacks on the stability and resilience of plant ecosystems, *Water Resour. Res.*, *42*, W01201, doi:10.1029/2005WR004444.

Ridolfi, L., P. D'Odorico, F. Laio, S. Tamea, and I. Rodriguez-Iturbe (2008), Coupled stochastic dynamics of water table and soil moisture in bare soil conditions, *Water Resour. Res.*, *44*, W01435, doi:10.1029/2007WR006707.

Rodriguez-Iturbe, I., P. D'Odorico, F. Laio, L. Ridolfi, and S. Tamea (2007), Challenges in humid land ecohydrology: Interactions of water table and unsaturated zone with climate, soil, and vegetation, *Water Resour. Res.*, *43*, W09301, doi:10.1029/2007WR006073.

Shampine, L., and M. Reichelt (1997), The MATLAB ODE suite, *SIAM J. Sci. Stat. Comput.*, *18*(1), 1–22.

Thorburn, P. (1997), Land management impacts on evaporation from shallow, saline water tables, in *Subsurface Hydrological Responses to Land Cover and Land Use Changes*, edited by M. Taniguchi, Kluwer Academic Publishers, Boston, Mass.

Thorburn, P., T. Hatton, and G. Walker (1993), Combining measurements of transpiration and stable isotopes of water to determine groundwater discharge from forests, *J. Hydrol.*, *150*(2–4), 563–587.

Troch, P. A., C. Paniconi, and E. E. van Loon (2003), Hillslope-storage Boussinesq model for subsurface flow and variable source areas along complex hillslopes: 1. Formulation and characteristic response, *Water Resour. Res.*, *39*(11), 1316, doi:10.1029/2002WR001728.

Tuteja, N. K., J. Vaze, B. Murphy, and G. Beale (2004), CLASS: Catchment scale multiple-landuse atmosphere soil water and solute transport model, *Tech. Rep. 01/12*, 51 pp., Cooperative Research Centre for Catchment Hydrology, Melbourne, Aust.

van de Koppel, J., and M. Rietkerk (2004), Spatial interactions and resilience in arid ecosystems, *Am. Nat.*, *163*(1), 113–121.

van Genuchten, M. (1980), A closed-form equation for predicting the hydraulic conductivity of unsaturated soils, *Soil Sci. Soc. Am. J.*, *44*(5), 892–898.

Vaze, J., N. K. Tuteja, and J. Teng (2004), CLASS: Unsaturated Moisture Movement Model U3M-1D Users's Manual, NSW Department of Infrastructure, Planning and Natural Resources, Australia and Cooperative Research Centre for Catchment Hydrology, 33 pp., Australia. (Available at http://www.toolkit.net.au/Tools/CLASS-U3M-1D/documentation)

von Hardenberg, J., E. Meron, M. Shachak, and Y. Zarmi (2001), Diversity of vegetation patterns and desertification, *Phys. Rev. Lett.*, *87*(19), 198,101.

Walker, B., D. Ludwig, C. Holling, and R. Peterman (1981), Stability of semi-arid savanna grazing systems, *J. Ecol.*, *69*(2), 473–498.

Walker, B., et al. (2002), Resilience management in social-ecological systems: A working hypothesis for a participatory approach, *Conserv. Ecol.*, *6*(1), 14.

Walker, B., C. S. Holling, S. R. Carpenter, and A. Kinzig (2004), Resilience, adaptability and transformability in social-ecological systems, *Ecol. Soc.*, *9*(2), 5.

Wigmosta, M., L. Vail, and D. Lettenmaier (1994), A distributed hydrology-vegetation model for complex terrain, *Water Resour. Res.*, *30*(6), 1665–1679.

Yu, B., C. W. Rose, K. J. Coughlan, and B. Fentie (1997), Plot-scale rainfall-runoff characteristics and modeling at six sites in Australia and southeast Asia, *Trans. ASAE*, *40*(5), 1295–1303.

Zhang, L., W. Dawes, P. Slavich, W. Meyer, P. Thorburn, D. Smith, and G. Walker (1999), Growth and ground water uptake responses of lucerne to changes in groundwater levels and salinity: Lysimeter, isotope and modelling studies, *Agric. Water Manage.*, *39*(2–3), 265–282.

R. M. Argent, Water Division, Bureau of Meteorology, GPO Box 1289, Melbourne, Vic 3001, Australia.

F. H. S. Chiew, CSIRO Land and Water, GPO Box 1666, Canberra, ACT 2601, Australia.

T. J. Peterson and A. W. Western, Department of Civil and Environmental Engineering, University of Melbourne, Parkville, Vic 3010, Australia. (peterson.tim.j@gmail.com)